OPEN ACCESS
IOP Publishing
Journal of Physics D: Applied Physics
J. Phys. D: Appl. Phys. **54** (2021) 285203 (9pp)
https://doi.org/10.1088/1361-6463/abf956

Measurement of the free electron line density in a spherical theta-pinch plasma target by single wavelength interferometry

P Christ[1,*], K Cistakov[1], M Iberler[1], L Laghchioua[1], D Mann[1], O Rosmej[2], S Savin[3] and J Jacoby[1]

[1] Institute of Applied Physics, Goethe University Frankfurt, 60438 Frankfurt am Main, Germany
[2] GSI Helmholtzzentrum für Schwerionenforschung GmbH, 64291 Darmstadt, Germany
[3] Institute for Theoretical and Experimental Physics, 117218 Moscow, Russia

E-mail: ph.christ@iap.uni-frankfurt.de

Received 1 January 2021, revised 23 March 2021
Accepted for publication 19 April 2021
Published 5 May 2021

Abstract

A single wavelength heterodyne interferometer has been set up to investigate the free electron density integrated axially along the line of sight (line density) in a theta-pinch plasma to determine its applicability as a plasma target for ion beam stripping. The maximal line density reached in this experiment was $(3.57 \pm 0.28) \times 10^{18}\,\mathrm{cm}^{-2}$ at 80 Pa and 20 kV. The findings demonstrate the pulsed character of the line density and its increase by raising the load voltage and the working gas pressure. Additionally, the results were compared with spectroscopic free electron density estimations, which were carried out by H_β-line broadening and peak separation. The time behavior of the line density indicates that its peak value is delayed by about 10 μs compared to the spectroscopic results. This effect is due to the formation of an extended, magnetically compressed plasma column in the vicinity of the current maximum, although the highest volumetric free electron density is reached near the current zero crossing. Since the line density is an essential parameter in describing the stripping capabilities of the plasma target, the interferometric diagnostic is superior to a spectroscopic diagnostic, because it directly provides integrated values along the line of sight. Furthermore, the measurements of the line density in this experiment partially show nonphysical negative values, which is due to gaseous effects and residual shot vibrations.

Keywords: interferometry, spectroscopy, line density, theta-pinch, plasma ion beam interaction

(Some figures may appear in colour only in the online journal)

* Author to whom any correspondence should be addressed.

1. Introduction

Interferometry is a powerful tool applied for plasma density measurements in the line of sight by simultaneously providing a high time resolution and a high accuracy. Since a free electron density measurement is one of the most essential diagnostic on a plasma, interferometry is widely applied for this purpose in experiments such as magnetic fusion devices, arc discharges and pulsed power devices like theta-pinchs [1–3]. Pinch devices have a long history in plasma physics since they were first candidates for magnetic fusion research [4].

Our theta-pinch devices, however, were developed to study ion beam plasma interaction for ion beam stripping [5–8]. When an ion beam interacts with a fully ionized plasma target, collisions of the projectile with free plasma particles (electrons and ions) lead to a stripping of the projectile electrons [9, 10]. The more collisions the projectile encounters on its path through the plasma target, the more does the effective charge state increase [9, 11]. After a certain propagation path length in the plasma target, the projectile attains an equilibrium charge state, at which the cross sections of ionization and recombination processes for the projectile are equal [9, 10]. Moreover, in a cold gas target, the total recombination cross section is dominated by the cross section of the bound electron capture, which is reduced by several orders of magnitude in a fully ionized plasma leading to an higher charge state [9]. A detailed overview of the atomic processes is given in [12]. As a fully ionized plasma target is necessary, hydrogen is used as the working gas. It is fully ionized (>99%) above a temperature of 3 eV at a density of $10^{17}\,\mathrm{cm}^{-3}$. Since free electron and ion densities match in a hydrogen plasma, the free electron line density and the effective plasma ionization degree defined by the fraction of the line densities of free electrons and neutral gas atoms are the most essential parameters for characterizing the plasma target regarding its stripping capabilities. Interferometry offers the most convenient approach for measuring these parameters since it intrinsically provides an integrated measurement along the line of sight. Additionally, the line densities of free electrons and neutral gas atoms could be separated by using two wavelengths.

Spectroscopic methods like line broadening and line intensity ratios, however, which have always been our diagnostic approach, can only provide the number of free electrons per volume. From such a measurement, a line density is not easily derived since a theta-pinch plasma is inhomogeneous and changes its geometric dimensions rapidly [13]. Furthermore, for an actual neutral particle density and ionization degree measurement, respectively, a supporting electron temperature estimation is necessary [14]. This is also quite challenging, since the line intensity ratio technique requires an assumption on the plasma state, which might also change in time. For example, the validity of common criteria for a prevalent local thermal equilibrium is violated in the ionization phase of a theta-pinch plasma [15–18]. In addition, if full ionization of the hydrogen plasma would be attained, spectroscopy by line emission can not be used. Consequently, a different technique, e.g. continuum radiation observation or plasma doping could be utilized [14, 19]. Collisional-radiative modeling could improve the spectroscopic approach significantly, but the spatial inhomogeneity of the plasma along the total axis could lead to erroneous line density results from such model and high effort is necessary to model this plasma in space and time appropriately.

In order to bypass these spectroscopic obstacles and resolve the lack of a proper, direct free electron line density and plasma ionization degree measurement at our plasma targets, an interferometric set-up was developed. Moreover, a new theta-pinch set-up was built and tailored for an interferometric performance. In a first step described in this work, the interferometer is run by a single wavelength to test its applicability, especially when dealing with high electromagnetic noise, and to get a first impression of the magnitude of the line density and its temporal behavior.

2. Theory

2.1. Interferometry

The physical principle which upon a interferometer can be utilized for a plasma density measurement is that a plasma posses a refractive index which depends on the predominant densities of free and bound electrons [20]:

$$(N-1)_p = \sum_i (N-1)_i = \sum_i \alpha_i n_i \tag{1}$$

N is the refractive index, α_i and n_i are the dynamic polarizability and the density of the ith species, respectively.

In an atmospheric plasma with highly populated excited states, it was shown that excited states can be neglected within an error 1.5 % [21]. Consequently, only the free electron and the neutral atom contributions are considered in the sum of equation (1) for a hydrogen plasma. The free electron contribution is given numerically by

$$(N-1)_e \approx -4.48 \times 10^{-28}\,\frac{\mathrm{cm}^3}{\mathrm{nm}^2}\,\lambda^2 n_e, \tag{2}$$

and λ is the wavelength of the light interacting with the plasma. Similarly, the polarizability was calculated for neutral hydrogen atoms and molecules [22]. Since the wavelength dependence is quite small, a mean value was taken between 400 and 700 nm for ground state hydrogen from the data in [22]:

$$(N-1)_H \approx 3.5 \times 10^{-24}\,\mathrm{cm}^3\, n_H\,. \tag{3}$$

The influence of molecular hydrogen is quite little, because the refractive index of molecular hydrogen is about twice of that of atomic hydrogen [22].

Since the particle densities may temporally evolve in a plasma, the resulting change of the refractive index can be measured interferometrically. The change of the refractive index leads to a phase shift according to

$$\Delta\varphi = \frac{2\pi}{\lambda}\int (N-1)_p\, dl\,. \tag{4}$$

If a single wavelength interferometer is used and the refractive index of the plasma is considered to be equal to only the

electron contribution, the free electron line density can be evaluated as

$$\int n_e \, dl = \frac{\Delta\varphi}{2\pi C_e \lambda}. \tag{5}$$

The constant C_e is the numeric value in equation (2) in an appropriate unit.

The phase shift $\Delta\varphi$ is extracted by using a heterodyne technique by comparing the detector signal with a stationary reference signal [23, 24]. Then, two voltages

$$U_I = \cos(\Delta\varphi) \tag{6}$$

$$U_Q = \sin(\Delta\varphi), \tag{7}$$

are resulting from a proper signal processing [25, 26] and the phase shift can be calculated according to

$$\Delta\varphi = \arctan\left(\frac{U_Q}{U_I}\right). \tag{8}$$

2.2. Spectroscopy

The most common approach to measure the free electron density spectroscopically is to evaluate the full width at half maximum (FWHM) of a hydrogen line and to compare it with calculated values for which different combinations of electron densities and electron temperatures were used [15, 27–29]. In this context, the hydrogen balmer beta (H_β) transition offers the most convenient opportunity for a pure free electron density estimation, because it is quite sensitive to the Stark-effect and its temperature dependence is quite low [30, 31]. Consequently, the free electron density can directly be evaluated from the FWHM $\Delta\lambda_{1/2}$ [9]:

$$n_e = 1.03 \times 10^{16} \left(\Delta\lambda_{1/2}\right)^{1.488}. \tag{9}$$

The numeric value is chosen in a way that the FWHM has the unit (nm) and the free electron density the unit (cm^{-3}).

In this procedure, the FWHM is extracted by a Voigt-fit and its Lorentzian width is sufficient for representing the FWHM to perform an free electron density calculation [31, 33]. The Gaussian contribution is generated by instrumental and Doppler broadening and the latter tends to be only significant at low density/high temperature plasmas, which is not the case in this work. Furthermore, ion dynamics play only a role for the central dip of the H_β-line, but do not alter the FWHM [28, 32].

Besides the investigation of the FWHM, the central line structure of the H_β-line can also be used for a free electron density measurement. Since its profile posses no pure Gauß- or Lorentz-contributions, but is rather strongly influenced by the Holtsmark-function, the central region of the H_β-line may exhibit two asymmetric peaks [33–36]. The distance between these two peaks $\Delta\lambda_{ps}$ has been examined for its applicability as a free electron density diagnostic tool and an empiric formula was derived [33]:

$$\Delta\lambda_{ps} = 1.32 \left(\frac{n_e}{10^{17}}\right)^{0.61 \pm 0.03}. \tag{10}$$

As in equation (9), the units are (cm^{-3}) for the free electron density and (nm) for the peak separation. The peak positions can be extracted by either smoothing the measured profile or by an actual line profile fit [33, 36].

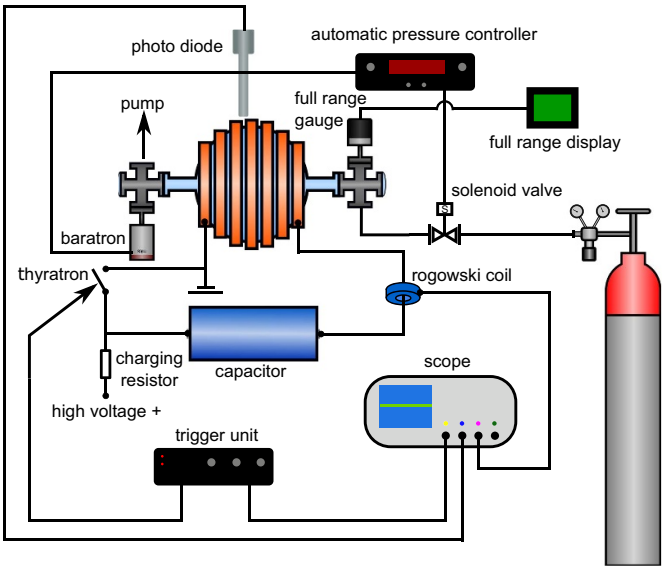

Figure 1. Schematic theta-pinch set-up.

3. Experimental set-up

3.1. Theta-pinch set-up

In figure 1, a schematic overview of the theta-pinch set-up is displayed. As can be seen, the theta-pinch consists of a capacitor bank, which has 30 μF capacitance, and a coil, which has 7.5 μH inductance, forming a damped resonant circuit at 10.5 kHz. The load voltage of the capacitor bank reaches a maximum value of 20 kV, which leads to a total stored energy of 6 kJ. When the theta-pinch is ignited, a current up to 40 kA is achieved.

A vessel is placed inside the coil, which contains hydrogen gas of about 20–80 Pa pressure and the total length of the vessel and the connected vacuum components along the axis is about 94 cm. Due to the alternating magnetic field, an induced electric field acts on the working gas and energy is coupled in by accelerating free electrons. If the mean free path length of the electrons is sufficient to gain the ionization energy by this acceleration, an avalanching process is initiated and a plasma is formed by collisional ionization [37]. The azimuthal plasma current and the axial magnetic field produce a Lorentz-force pinching the plasma to the coil axis and a high free electron density is achieved [37].

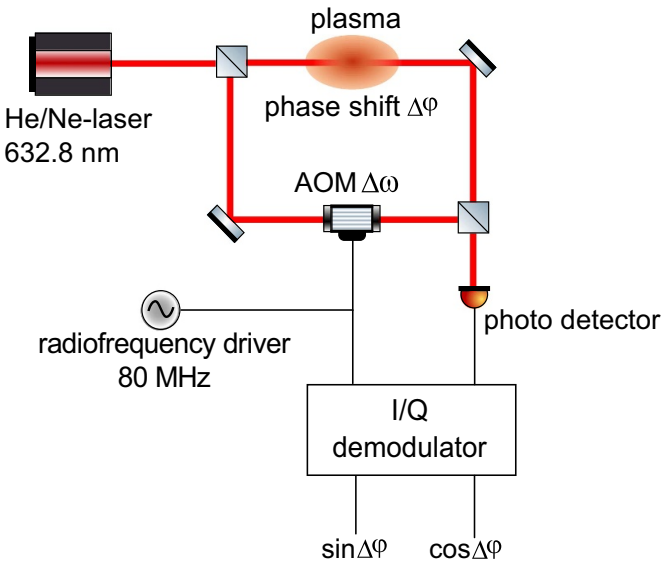

Figure 2. Schematic heterodyne single wavelength interferometer set-up.

Additional supporting diagnostic tools are used on this set-up, e.g. a photo diode monitoring the plasma light emission in the visible region, a rogowsky-coil for a current measurement and a baratron for a precise pressure setting.

3.2. Single wavelength interferometer

Figure 2 shows the single wavelength interferometric set-up schematically [38]. This heterodyne Mach–Zehnder interferometer is run by a helium/neon-laser, which posses an output power of 21.5 mW. The frequency shift is produced by an acousto-optic modulator and its value of 80 MHz sets a lower limit of 12.5 ns to the time resolution. This 80 MHz carrier is eliminated by 30 MHz low pass filters at the outputs of the I/Q-demodulator. Before using equation (8), deviations from the ideal equations (6) and (7) resulting from imperfect electrical components in the I/Q-demodulator are corrected by calibration procedures [25, 26, 38]. Additionally, all electrical components used in this set-up are contained inside a Faraday cage to shield them from the electromagnetic noise produced during the discharge.

3.3. Spectroscopic set-up

The spectroscopic set-up consists of a monochromator (Jobin-Yvon-HR2), a CCD-camera (PCO Sensicam) and a fiber. The fiber is placed end-on to have an axial line of sight. The monochromator selects the H_β-line, which is recorded by the CCD-camera. The pixel to wavelength conversion is achieved by adding argon to the hydrogen in a separated measurement. In the vicinity of the H_β-line, two to three strong argon lines are visible, whose central wavelengths are known and can be utilized for a calibration. In this way, a value of 5.035 pm/pixel was derived. The instrumental broadening caused by the optical system, e.g. by the slits of the monochromator, has a value of 0.136 nm and was measured by a very weak argon discharge. Then, the argon line widths are only dominated by the broadening by the optical system since they do not exhibit a linear Stark-effect [39]. The Doppler-broadening of these argon lines is negligible due to the low temperature in a weak discharge and the high mass of the argon ions. In hydrogen, the Doppler-broadening of the H_β-line is at 0.037 nm at $T = 1$ eV. In argon, this broadening is about six times lower at the same temperature since the temperature/rest mass ratio is smaller by a factor of 40.

4. Experimental results and discussion

The free electron line density was measured in the range of 20–80 Pa at load voltages from 12 to 20 kV by interferometry. The results were averaged over 20 shots for each combination of these parameters except for 40 Pa/12 kV. At these parameters, the plasma ignited irregularly and only four shots were averaged. The results will emphasize more on the shot conditions 40 Pa/18 kV, because this a typical pressure applied with our current plasma stripper prototype and the data will provide good comparison with further interferometric diagnostics on that experiment. Additionally, at the theta-pinch described in this work, the energy transfer efficiency into the plasma is best at 18 kV.

Figure 3 exemplarily shows the interferometric results for a pressure of 40 Pa. It can be seen, that the higher the load voltage, the earlier is the peak free electron line density reached and the higher is its value. Moreover, the curves demonstrate the pulsed character of this theta-pinch plasma. In general, early cycles, which show no ignition, function as a pre-ionization by producing enough free charge for a drastic ignition in one the following cycles. By increasing the load voltage, the induced electrical field increases accordingly and the pre-ionization process is enhanced leading to an earlier ignition. The peak value is not reached right after ignition, but in a later cycle, where the cumulative energy input to magnetic compression force ratio is optimal.

Furthermore, figure 3 shows nonphysical negative density values, which appear as spikes at the zero crossings of the current at the beginning of the discharge and as an offset from around 0.6 ms to the end of the discharge, except for the 12 kV results. However, the 12 kV results can be used to find the origin of the negative density values. In figure 4, the average phase shift from five shots at 12 kV and 40 Pa, which did not achieve an ignition, is displayed. This data also exhibits fast spikes at the beginning of the discharge and then showing a transition to an oscillating behavior. In principle, the single wavelength interferometer is incapable of distinguishing between different particle species present in the plasma. For the evaluation of the data in this work, only free electrons are considered since their contribution to the refractive index is about a factor of 100 higher than that of the neutral gas for wavelengths around 1 μm as shown by equations (2) and (3). But the free electron and neutral atom contributions have opposite signs. Consequently, if the discharge is weak, gaseous effects are not covered up by the electron contribution leading to negative values at the beginning of the

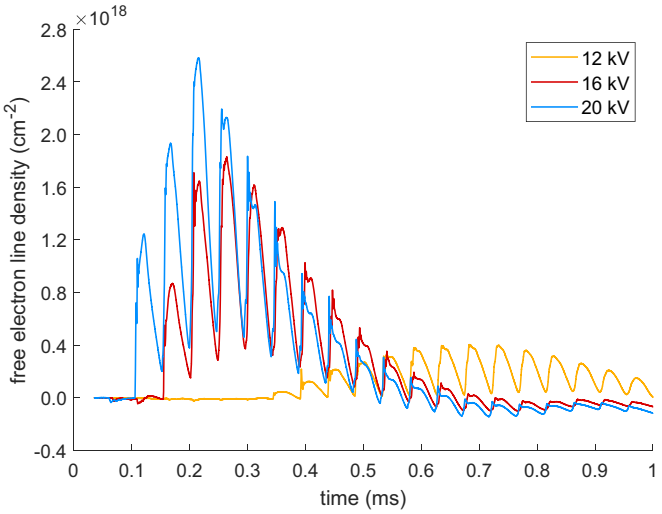

Figure 3. Free electron line density at 40 Pa at different load voltages.

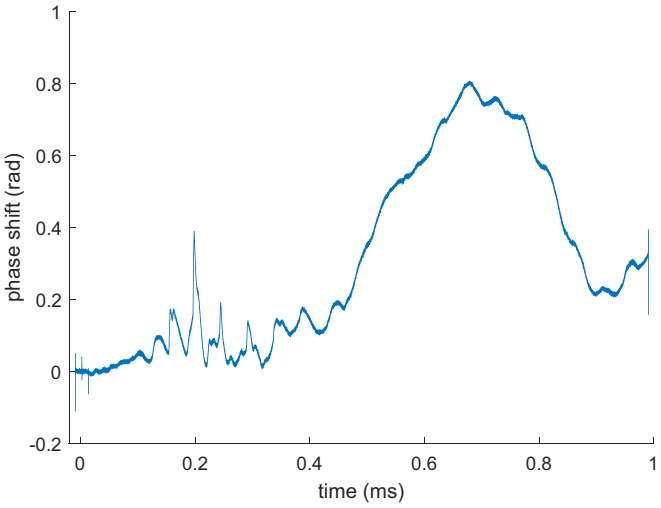

Figure 4. Average phase shift from five failed ignitions at 12 kV and 40 Pa showing gaseous effects from 0 to 0.4 ms and significant residual shot vibrations from 0.4 to 1 ms.

discharge. The low frequency oscillating behavior, starting at around 0.4 ms and peaking between 0.6 and 0.8 ms, is caused by residual shot vibrations in the data, when vibrations from the pulsed power system are transferred to the interferometric system after the onset of the current. For resolving this problem, a vibration isolation of the interferometer or a good statistic is necessary. This behavior is expected for all shot conditions and to increase by raising the load voltage. However, the region of interest is at the highest free electron line density values around 0.2 to 0.3 ms after the onset of the current and the offset-like error due to shot vibrations should be well within 2 rad in this temporal area. An error of 2 rad is equal to an error of about $1.1 \times 10^{17}\,\mathrm{cm}^{-2}$ in the line density. The further errors of the measurement consist of a systematic error of the order $10^{15}\,\mathrm{cm}^{-2}$ produced by the oscilloscope and the data processing and a statistic error from the averaging of around $10^{17}\,\mathrm{cm}^{-2}$. The statistic error includes the shot-to-shot variability of the data taking into account the reproducibility of the plasma and the variations in the residual shot vibrations. Low frequency vibrations can be neglected since they can be assumed constant for measurement duration.

Figure 5 gives an overview over the global maximal free electron line density values for all combination of shot conditions, which achieved an ignition. The highest free electron line density reached in this experiment was $(3.57 \pm 0.28) \times 10^{18}\,\mathrm{cm}^{-2}$ at 80 Pa and 20 kV. Additionally, figure 5 shows an increase of the free electron line density by raising the working gas pressure and/or raising the load voltage. Nevertheless, the results for a pressure of 20 Pa are clearly showing a region of saturation at high voltages. This saturation can be explained by the load voltage having already passed an optimal pressure/-voltage ratio [7, 13]. Unfortunately, this characteristic can not be investigated further at the higher end of the pressure range, because the electrical system regarding the load voltage is limited to 20 kV. Additionally, the data points in the low voltage range seem not to be sufficient to draw a reliable conclusion, whether this is a general behavior. Indeed, the 40 Pa trend line

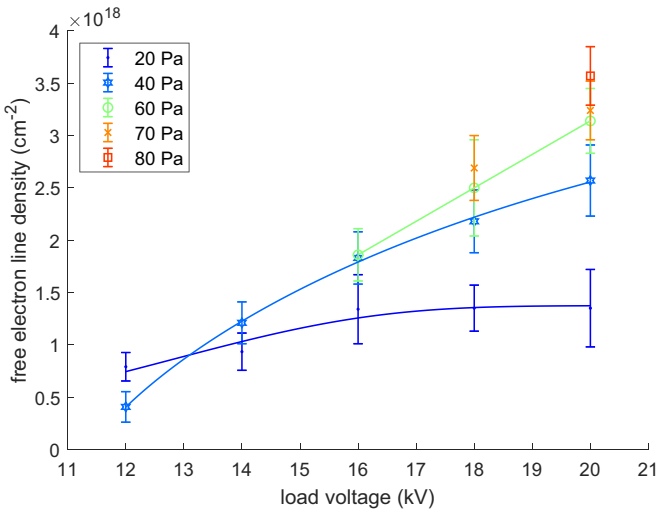

Figure 5. Maximal free electron line density values at different combinations of pressure and load voltage. Additional trend lines are shown for 20, 40 and 60 Pa.

may indicate a saturation being achieved at higher voltages, but the 60 Pa values behave highly linear, although three data points do not provide high confidence there.

For comparison, a spectroscopic diagnostic was carried out at 40 Pa and 18 kV. In this measurement, the free electron density was derived by Stark-broadening as well as by peak separation according to equations (9) and (10). The latter can only be used if the line posses two distinct peaks, but this characteristic disappears at low densities [33]. The error of the Stark-broadening method is around 10% and that of the peak separation method is given in equation (10). Since the peaks were extracted by line smoothing, an additional uncertainty from the smoothing algorithm must be taken into account. To increase the precision, the algorithm discards a line which is still too jagged even after smoothing, e.g. if more than one central dip

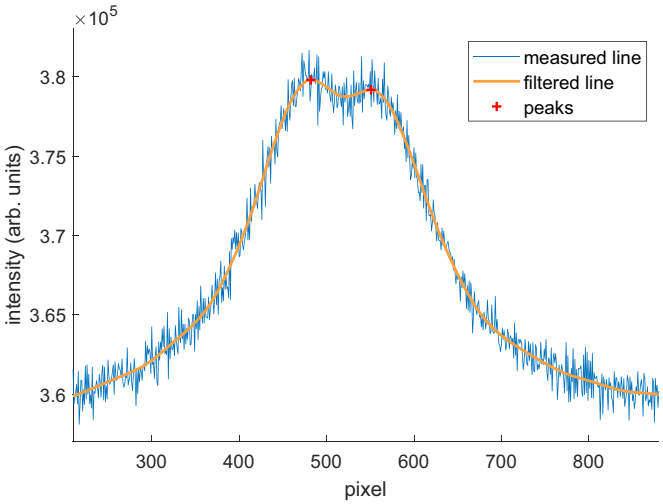

Figure 6. Example of a measured H_β-line for the spectroscopy at 40 Pa and 18 kV at 170.2 μs delay.

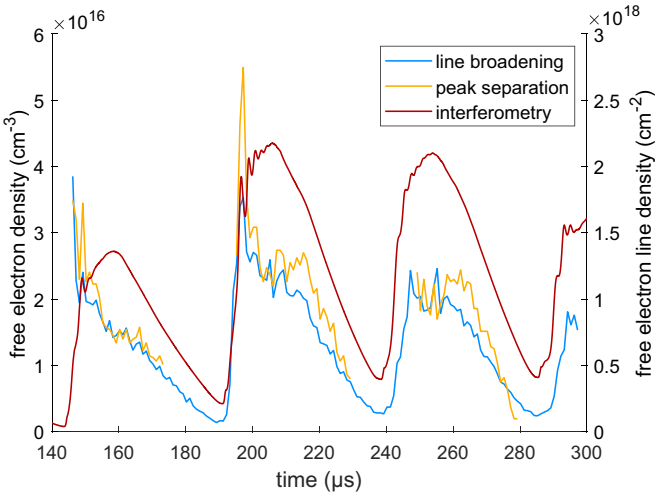

Figure 7. Temporal behavior of the free electron densities at 40 Pa and 18 kV obtained by H_β-line broadening and H_β-peak separation compared to the free electron line density obtained from interferometry.

position are registered. The smoothing algorithm is a combination of wavelet denoise at level 5 and a Savitzky–Golay filter of the order 3 using 81 grid points [40]. Figure 6 exemplary demonstrates a H_β-line recorded for the spectroscopy and the concerning filtered line and the central peaks. The exposure used by the CCD-camera was set to 0.5 μs. The x-axis is scaled in pixels, since the spectroscopic system was not calibrated for absolute wavelength values, but only for the pixel/nm conversion. Concerning the line shape, the central dip may also be caused by optical thickness of the H_β-line. Whether the profile is influenced by self-absorption can be tested by comparing the free electron density obtained by the FWHM and by the peak separation method [41].

Figure 7 summarized the interferometric and spectroscopic results for the discharge condition 40 Pa/18 kV. The temporal evolution of the spectroscopic results were composed from single shots, which were separated by 1.0 μs. In the temporal area shown in figure 7, the plasma reproducibility only changes the amplitudes of the data, but the total temporal evolution remains the same. The overall behavior of both spectroscopic approaches are in good agreement, which is a clear sign for no significant self-absorption of the H_β-line. As indicated by figure 7, both spectroscopic approaches show narrow but high and synchronized free electron density peaks in the first two half cycles. Contrary, the free electron line density peak is delayed by about 10 μs in that half cycles. Interestingly, these sharp spectroscopic peaks are also reflected in the interferometric measurements by similar narrow peaks, but the maximal values are reached afterwards. The spectroscopic and interferometric measurements were not taken simultaneously, since both need access to an axial line of sight. A synchronization, however, was achieved by using each corresponding current signal as a clock. Unfortunately, these clocks are not stable in frequency as the plasma functions as a time dependent load alternating the frequency. Consequently, although the starting points of the current signals were matched, a synchronization uncertainty of about 1.5 μs occurs in the temporal window of figure 7. Nevertheless, the temporal difference between the density peaks is still significant. A contribution to this difference could be the way the light is collected for the spectroscopy. Although the fiber is directed along the axis, it has a certain acceptance angle, which introduces a spatial averaging of regions outside the central axis. Consequently, spectroscopy and interferometry do not monitor equal regions in this specific configuration. Nevertheless, in an experiment, in which a collimating lens in front of the fiber as well as diaphragms were used, a similar time behavior of the spectroscopic results occurred showing comparable narrow density peaks [13].

To understand the discrepancy between the interferometric and spectroscopic results concerning the occurrence of each maximal density value, an analysis of the temporal behavior of the discharge is useful. For this purpose, a CCD-camera was targeted at the vessel to record the plasma shape. The exposure was set to 0.5 μs again. The images for selected delays from the current starting point are displayed in figure 8.

Frame (a) shows a bright sphere-like but inhomogeneous pinch of the plasma in the center of the vessel. This time coincides with the peak spectroscopic free electron density in the first visible full cycle in figure 7. Frame (b) indicates a kind of disrupted shape caused by the plasma being axially ejected and partially colliding with the vessel due to the lack of a sufficient confinement on both sides to withstand the compression. This ejection is more clearly demonstrated in an earlier experiment [13]. The free electron density has already strongly decreased at this point, but the free electron line density is still on a rising slope. Frame (c) corresponds with the peak free electron line density. As can be seen, the radius of the column has further contracted and the emission indicates a more homogeneous density distribution. It seems that the elongated plasma column created by the ejection more than compensates the decreased free electron density leading to a free electron line density peak. From this point on, both the spectroscopic and

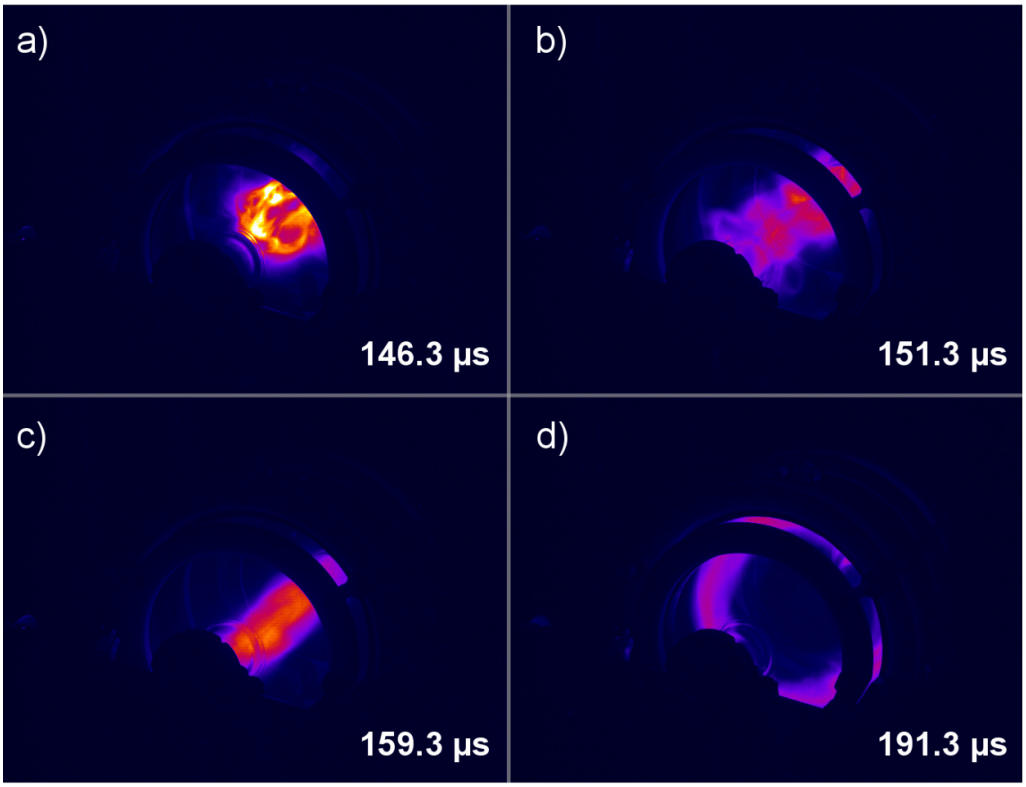

Figure 8. Images of the plasma shape at 40 Pa and 18 kV at different delays: (a) bright sphere-like pinch showing a local maximal free electron density, (b) ejected plasma column colliding with the vessel and being disrupted, (c) homogenized and compressed plasma column at local maximal free electron line density, (d) ring-like ignition in the next cycle showing only a remaining thin plasma near the center at minimal spectroscopic and interferometric values.

interferometric results decrease further as the plasma starts to diffuse and recombine. Thereafter, frame (d) presents the ring-like ignition at the beginning of the next cycle. Since there is only a thin plasma remaining on the central axis, both diagnostic approaches show a synchronized minimal density at this point.

5. Conclusion and outlook

The interferometric set-up used in this experiment has shown its applicability to measure the free electron line density in this theta-pinch plasma. Our former and current similar theta-pinch experiments, which were constructed to investigate plasma ion beam interaction for ion beam stripping, have always relied on spectroscopic diagnostics and lacked a time-resolved, line density measurement. This work provides the first directly measured free electron line density values in the context of the plasma stripper research in an inductively coupled plasma target by interferometry. From these measurements, significant information is provided on the time evolution and the range of the absolute values of free electron line density of this plasma.

Since the line densities of free electrons and neutral gas atoms are the crucial parameters for characterizing the plasma target concerning its stripping properties, the interferometric approach described here is superior to a spectroscopic approach, because it directly provides the line integrated values. As this theta-pinch plasma appears to be inhomogeneous and the length of the plasma column changes rapidly, an estimation of a line density from a spectroscopic free electron density measurement is highly inaccurate. Moreover, it was shown, that the peak values of both approaches do not match temporally and the interferometric peak results are delayed by about 10 μs. Consequently, using the spectroscopic data for choosing the temporal range for the ion beam plasma interaction is inaccurate and the interferometric results must be used. Furthermore, although anticipated, the time evolution of the free electron line density reflects the pulsed character of the experiment, which is an undesired property for ion beam stripping, since the ion beam will be stripped non-uniformly. However, compared to the coarse estimations in an earlier investigation [42], the free electron line density is increased by one order of magnitude in this experiment to values above $10^{18}\,\mathrm{cm}^{-2}$.

The next step regarding this research will be an upgrade of the interferometer by a second wavelength. In this way, the line density of the neutral gas could be measured directly and the effective ionization degree along the coil axis could be derived by the fraction of the line densities of free electron and neutral gas atoms. Consequently, a complete diagnostic of the stripping properties would be achieved. But already from the data provided in this work, we can conclude that the free electron line density must be further increased. For having universal stripping properties, a value of above $10^{20}\,\mathrm{cm}^{-2}$ is desired [9]. Nevertheless, a free electron line density of

around 3.5×10^{18} cm^{-2} is already sufficient to compete with foil strippers in a 20 MeV Pb-ion beam [11]. However, for raising the charge state, for example, of an uranium ion beam at 1.4 MeV u^{-1} significantly, an increase of the free electron line density of one order of magnitude is necessary [43, 44]. Furthermore, a change of the electrical circuit is also required to prolong the discharge to provide a uniform stripping for several 10 μs.

Data availability statement

The data that support the findings of this study are available upon reasonable request from the authors.

Acknowledgments

The authors want to thank the German Ministry for Education and Research (BMBF) for funding this research under Contract No. 05P18RFRB1. Additionally, P Christ is grateful for being supported by a scholarship from Helmholtz Graduate School for Hadron and Ion Research (HGS-HIRe).

ORCID iDs

P Christ https://orcid.org/0000-0002-7900-675X
O Rosmej https://orcid.org/0000-0003-0447-3510

References

[1] Kornejew P, Hirsch M, Bindemann T, Dinklage A, Dreier H and Hartfuß H-J 2006 Design of multichannel laser interferometry for W7-X *Rev. Sci. Instrum.* **77** 10F128
[2] Baum D, Hackmann J and Uhlenbusch J 1975 Interferometric measurement of particle densities in cascaded arcs at atmospheric pressure *Plasma Phys.* **17** 79–87
[3] Kuepper F P 1963 The change with time of the radial electron density distribution in theta pinch *Z. Naturforsch. (West Germany) Divided into Z. Nat.forsch. A and Z. Nat.forsch.* B **18a** 895–900
[4] Allen J 1958 Thermonuclear power and the pinch effect *Endeavour* **17** 117–26
[5] Teske C, Jacoby J, Senzel F and Schweizer W 2010 Energy transfer efficiency of a spherical theta pinch *Phys. Plasmas* **17** 043501
[6] Teske C, Liu Y, Blaes S and Jacoby J 2012 Electron density and plasma dynamics of a spherical theta pinch *Phys. Plasmas* **19** 033505
[7] Loisch G *et al* 2014 Review of the state-of-the-art development of the spherical theta pinch plasma source *IEEE Trans. Plasma Sci.* **42** 1163–72
[8] Xu G, Hock C, Loisch G, Xiao G, Jacoby J, Weyrich K, Li Y and Zhao Y 2015 New model of calculating the energy transfer efficiency for the spherical theta-pinch device *Phys. Plasmas* **22** 052703
[9] Peter T and Meyer ter Vehn J 1991 Energy loss of heavy ions in dense plasma. II. Nonequilibrium charge states and stopping powers *Phys. Rev.* A **43** 2015–30
[10] Peter T, Arnold R and Meyer ter Vehn J 1986 Influence of dielectronic recombination on fast heavy-ion charge states in a plasma *Phys. Rev. Lett.* **57** 1859–62
[11] Alton G D, Sparrow R A and Olson R E 1992 Plasma as a high-charge-state projectile stripping medium *Phys. Rev.* A **45** 5957–63
[12] Yu Tolstikhina I and Shevelko V P 2018 Influence of atomic processes on charge states and fractions of fast heavy ions passing through gaseous, solid and plasma targets *Phys.-Usp.* **61** 247–79
[13] Loisch G, Xu G, Blazevic A, Cihodariu-Ionita B and Jacoby J 2015 Hydrogen plasma dynamics in the spherical theta pinch plasma target for heavy ion stripping *Phys. Plasmas* **22** 053502
[14] Kunze H-J 2009 *Introduction to Plasma Spectroscopy* (Berlin: Springer)
[15] Griem H R 1964 *Plasma Spectroscopy* (New York: McGraw-Hill)
[16] Fujimoto T and McWhirter R W P 1990 Validity criteria for local thermodynamic equilibrium in plasma spectroscopy *Phys. Rev.* A **42** 6588–601
[17] Hey J D, Chu C C and Rash J P S 1999 Partial local thermal equilibrium in a low-temperature hydrogen plasma *J. Quant. Spectrosc. Radiat. Transfer* **62** 371–87
[18] Engelhardt W, Köppendörfer W and Sommer J 1971 Lack of partial thermal equilibrium in pinch discharges *Z. Phys.* A **246** 29–42
[19] Arad R, Ding L and Maron Y 1998 Novel gas-doping technique for local spectroscopic measurements in pulsed-power systems *Rev. Sci. Instrum.* **69** 1529–33
[20] Alpher R A and White D R 1965 Optical interferometry *Plasma Diagnostic Techniques* ed R H Huddlestone and S L Leonard (New York: Academic)
[21] Helbig V and Nick K-P 1992 Influence of excited atoms on the plasma refractivity *Contrib. Plasma Phys.* **32** 515–21
[22] Fulghum S F 1994 Multi-Beam Laser Interferometer for Plasma Density Measurements in a Plasma Erosion Opening Switch (PEOS) *Technical Report*, Science Research Laboratory, Inc
[23] Hutchinson I H 2005 *Principles of Plasma Diagnostics* (Cambridge: Cambridge University Press)
[24] Choi J-Y, Takano N, Urabe K and Tachibana K 2009 Measurement of electron density in atmospheric pressure small-scale plasmas using CO_2-laser heterodyne interferometry *Plasma Sources Sci. Technol.* **18** 035013
[25] Geng Z, Pengda G, Hou Mi and Pei G 2006 Design and calibration of a phase and amplitude detector *Proc. 2005 Particle Conf* (IEEE) (https://doi.org/10.1109/PAC.2005.1591798)
[26] Sabah S and Lorenz R 1998 Design and calibration of IQ-mixers *6th European Particle Conf. (EPAC 98)* pp 1589–91
[27] Kepple P and Griem H R 1968 Improved Stark profile calculations for the hydrogen lines Hα, Hβ, Hγ and Hδ *Phys. Rev.* **173** 317–25
[28] Gigosos M A and Cardeñoso V 1996 New plasma diagnosis tables of hydrogen Stark broadening including ion dynamics *J. Phys. B: At. Mol. Opt. Phys.* **29** 4795–838
[29] Touma J E, Oks E A, Alexiou S and Derevianko A 2000 Review of the advanced generalized theory for Stark broadening of hydrogen lines in plasmas with tables *J. Quant. Spectrosc. Radiat. Transfer* **65** 543–71
[30] Griem H R 2005 *Principles of Plasma Spectroscopy* (Cambridge: Cambridge University Press)
[31] Gigosos M A, Gonzalez M A and Cardenoso V 2003 Computer simulated Balmer-alpha, -beta and -gamma Stark line profiles for non-equilibrium plasmas diagnostics *Spectrochim. Acta* B **58** 1489–504

[32] Fleurier C, Sanba A, Hong. D, Mathias J and Pellicer J C 1988 Plasma diagnostics in the heavy ion beam-dense plasma interaction experiment at Orsay *J. Phys. Colloques* **49** C7–141–C7–149
[33] Surmick D and Parigger C 2014 Empirical formulae for electron density diagnostics from H_α and H_β line profiles *Int. Rev. At. Mol. Phys.* **5** 73
[34] Griem H R 1974 *Spectral Line Broadening by Plasmas* (New York: Academic)
[35] Henri V R 1965 Spectral line broadening *Annu. Rev. Astron. Astrophys.* **3** 71–92
[36] Žikić R, Gigosos M A, Ivković M, González MA and Konjević N 2002 A program for the evaluation of electron number density from experimental hydrogen Balmer beta line profiles *Spectrochim. Acta* B **57** 987–98
[37] Sato M 1962 Particle acceleration and breakdown conditions in an alternating magnetic field *Il Nuovo Cimento (1955-1965)* **23** 22–46
[38] Christ P 2017 Aufbau und Test eines heterodynen Interferometers zur zeitaufgelösten Bestimmung der Elektronendichte an einem Plasmastripper Master's Thesis Goethe University Frankfurt
[39] Bohlender B 2019 Entwicklung und plasmaphysikalische Untersuchung eines Plasmafensters zur Erzeugung hoher Druckunterschiede PhD Thesis Goethe University Frankfurt
[40] Press W H, Teukolsky S A, Vetterling W T and Flannery B P 2002 *Numerical Recipes in C++ - The Art of Scientific Computing* (Cambridge: Cambridge University Press)
[41] Ivković M, Konjević N and Pavlović Z 2015 Hydrogen Balmer beta: the separation between line peaks for plasma electron density diagnostics and self-absorption test *J. Quant. Spectrosc. Radiat. Transfer* **154** 1–8
[42] Loisch G 2014 ZeitaufgelösteWasserstoffplasma-Diagnostik am Sphärischen Theta Pinch Master's Thesis Goethe University Frankfurt
[43] Hoffmann D H H, Weyrich K, Wahl H, Gardés D, Bimbot R and Fleurier C 1990 Energy loss of heavy ions in a plasma target *Phys. Rev.* A **42** 2313–21
[44] Shevelko V 2015 personal communication